Proteome-wide Covalent Targeting of Acidic Residues with Tunable *N*-Aryl Aziridines

Nan Qiu,[1,2#] Hao Tan,[3#] Dany Pechalrieu,[1] Daniel Abegg,[1] Deepanshu Fnu,[1] Poulami Mukherjee,[3⊥] Angel Renteria Gomez,[3⊥] Osvaldo Gutierrez,[3⊥] David C. Powers,[3*] and Alexander Adibekian[1,4,5,6,7*]

[1] Department of Chemistry, University of Illinois Chicago, Chicago, IL 60607, USA

[2] Skaggs Graduate School and Chemical and Biological Sciences, Scripps Research, La Jolla, CA 92037, USA

[3] Department of Chemistry, Texas A&M University, College Station, TX 77843, USA

[4] Department of Pharmaceutical Sciences, University of Illinois Chicago, Chicago, IL 60612, USA

[5] Department of Biochemistry and Molecular Genetics, University of Illinois Chicago, Chicago, IL 60607, USA

[6] University of Illinois Cancer Center, Chicago, IL 60607, USA

[7] UICentre, University of Illinois Chicago, Chicago, IL 60612, USA.

[⊥] Present address: Department of Chemistry & Biochemistry, University of California, Los Angeles, Los Angeles, CA 951569 USA.

* Correspondence: aadibeki@uic.edu; powers@chem.tamu.edu

[#] These authors contributed equally.

Abstract

Carboxylate side chains in aspartic and glutamic acids play critical roles in protein structure and function due to their polarity and negative charge. These acidic residues, which are abundant in high-value drug targets, represent attractive yet underexplored hotspots for covalent inhibitor discovery. In this study, we introduce *N*-aryl aziridines as a systematically tunable, chemoselective scaffold for covalent targeting of carboxylates across the proteome. Using a library of *N*-pyridinium aziridine-based fragments combined with chemoproteomics-enabled target deconvolution, we identified lead hits for aspartates and glutamates in proteins such as mitochondrial carrier homolog 2 (MTCH2), RUN and FYVE domain-containing protein 1 (RUFY1), and delta(24)-sterol reductase (DHCR24). Modular *build-and-couple* synthetic logic enabled fragment evolution via Ni-catalyzed cross-coupling to access *N*-aryl aziridines with enhanced affinities for MTCH2 and RUFY1. Notably, *N*-aryl aziridine **5b** selectively modified RUFY1 at E502, disrupting its interactions within the endosomal trafficking network and impairing receptor recycling. This work establishes *N*-aryl aziridines as versatile carboxylate-targeting covalent inhibitor scaffolds, broadening the scope of covalent ligand discovery.

Main

Carboxylates, essential for numerous biochemical processes due to their polarity and negative charge, are among the most abundant and functionally diverse side chains in the proteome. In addition to their roles in protein structure, ligand binding, metal coordination, and acid-base catalysis,[1-3] aspartic (Asp) and glutamic (Glu) acids often stabilize protein complexes through electrostatic interactions, making them attractive yet underutilized targets for scaffolding proteins that lack enzymatic activity.[1, 4] Importantly, these residues can exhibit hyperreactivity within high-value drug targets. For example, aspartic proteases have been successfully targeted with small-molecule inhibitors for treating viral infections,[5] underscoring the therapeutic potential of catalytic carboxylic acids. While active-site carboxylates have been targeted to develop effective treatments, non-catalytic aspartate and glutamate residues represent an unexplored space for expanding the druggable proteome. Unlike active-site-directed antivirals, which depend on extensive non-covalent interactions,[6,7] covalent targeting provides a reactivity-driven approach

well-suited for selectively modifying non-catalytic residues. This strategy has been successfully employed to profile cysteine,[8-10] lysine,[11, 12] and tyrosine residues,[13, 14] illuminating the potential for covalent ligands to target carboxylate side chains. While earlier studies have demonstrated isolated cases of covalent carboxylate modification,[15-17] their broader utility in fragment-based drug discovery remains limited due to the lack of robust chemical methods for rapid ligand diversification or the reliance on light-activated ligands. Furthermore, examples extending beyond single protein targets have yet to be demonstrated. Furthermore, examples extending beyond single protein targets have not been realized, leaving a critical gap in the development of broadly applicable and synthetically tunable scaffolds. Developing a tunable and synthetically tractable scaffold to target acidic residues is thus critical for systematically unlocking previously undruggable targets by chemoproteomics.

Strained three-membered heterocycles, such as epoxides, aziridines, and oxaziridines, combine strain-enhanced reactivity with benchtop stability, making them attractive warheads for chemoselective bioconjugation and covalent inhibitor development.[18-21] While the protein reactivities of epoxides and oxaziridines have been extensively characterized for profiling reactive cysteines[22] and methionines,[23] respectively, aziridines remain largely uncharacterized for systematic proteome-wide ligand discovery applications. Early studies on cyclophellitol-based aziridines revealed potent, mechanism-based inhibition of β-exoglucosidases,[24] paving the way for activity-based probes to profile this enzyme family.[25, 26] More recently, the 1,2,3-trisubstituted aziridine compound RMC-9805 was developed as a tri-complex modality to target the oncogenic KRas G12D mutant, demonstrating durable tumor regressions in pancreatic cancer models.[27] These pioneering findings prompted us to hypothesize that aziridines could serve as tunable acid-directed warheads for proteome-wide covalent ligand discovery.

Herein, we present the development and chemoproteomic evaluation of *N*-aryl aziridines as a tunable scaffold for proteome-wide targeting of aspartic and glutamic acids, enabled by a modular *build-and-couple* approach (Fig. 1a). Using an *N*-aryl aziridine probe, we profiled proteome-wide carboxylate residues in live cancer cells, achieving ~70% chemoselectivity over other amino acids. Through competitive proteomic profiling of a small library of *N*-pyridinium aziridine fragments synthesized in a single chemical step (Fig. 1b), we identified fragments that ligated Asp and Glu residues in mitochondrial carrier homolog 2 (MTCH2), RUN and FYVE domain-containing protein 1 (RUFY1), and delta(24)-sterol reductase (DHCR24). These fragments were further diversified into *N*-aryl aziridines through a second chemical step, resulting in improved potency against MTCH2 and RUFY1. Finally, we demonstrate that targeting E502 in RUFY1 with *N*-aryl aziridine **5b** disrupts its interaction with scaffolding trafficking partners and impairs endosomal recycling of surface receptors, highlighting the pharmacological potential of targeting non-catalytic carboxylates.

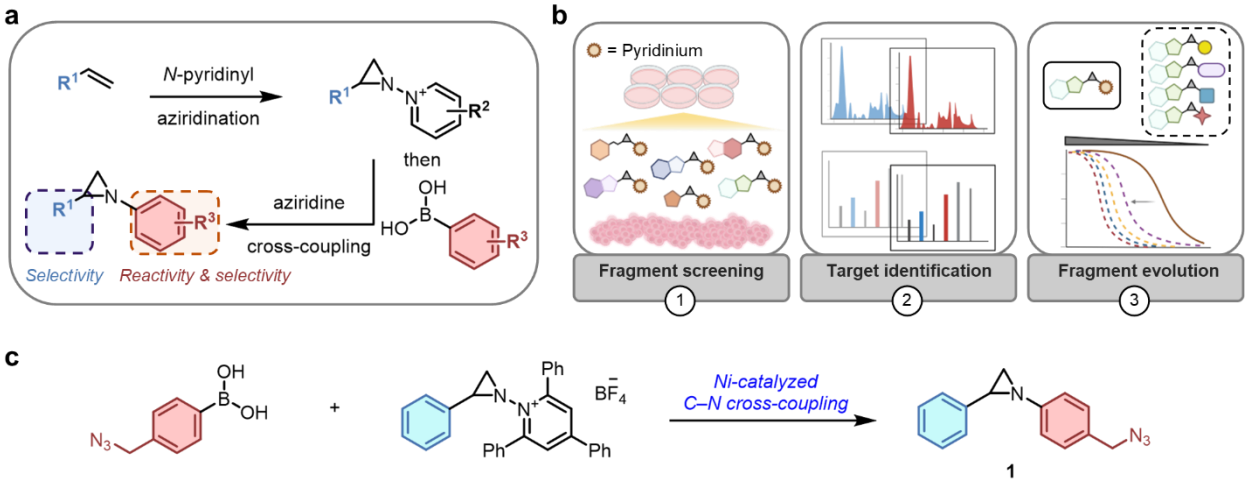

Figure 1. Conceptual representation of chemoproteomics-enabled *N*-aryl aziridine ligand discovery. (a) Synthetic scheme for the *build-and-couple* strategy to access disubstituted *N*-aryl aziridines. (b) Schematic workflow of fragment screening, target identification and fragment evolution to rapidly generate diverse *N*-aryl aziridine-based inhibitors. (c) Synthetic scheme of a simple disubstituted *N*-aryl aziridine azide probe **1**. Reaction conditions: Ni(phen)Br_2 (20 mol%), K_3PO_4 (2.8 equiv.), 2,4,6-collidine in MeCN (0.08 M, 1.0 equiv), 65 °C, 36 h.

Results

Synthesis and proteome-wide characterization of a disubstituted aryl aziridine probe. We began our studies by characterizing the protein reactivity of *N*-aryl aziridines. To this end, we synthesized a simple, clickable chemical probe, **1** (Fig. 1c), using the two step *build-and-couple* strategy comprised of olefin *N*-aminopyridylation followed by Ni-catalyzed C–N coupling that we recently reported.[28,29] Robust, concentration-dependent proteome labeling by **1** was observed in cellular lysates, confirming the aziridine as a broadly protein-reactive electrophile (Fig. S1). Probe **1** also exhibited efficient cellular uptake and live-cell labeling regardless of serum levels in the media, indicating minimal cross-reactivity with serum proteins (Figs. 2a, S2). Fluorescence microscopy images revealed significant protein modification in the nucleus and cytosol by **1** (Fig. 2a). Some naturally-occurring and synthetic aziridine-containing molecules, including mitomycin C, are known to be biologically active due to DNA alkylation via nucleophilic ring opening.[30] However, treatment with the unactivated *N*-aryl aziridine **2b** resulted in no detectable DNA damage in cells (Fig. S3).

Next, we evaluated the chemoselectivity and chemical identity of the protein adducts formed by probe **1**. Briefly, HCT116 cells were treated with 100 µM of **1** for 4 hours, followed by conjugation of the labeled proteins to desthiobiotin alkyne after cell lysis. After tryptic digestion, the probe-modified peptides were enriched using streptavidin and analyzed by LC-MS/MS. Using FragPipe open search,[31] we identified a single unique mass adduct (+458.2798 Da) exclusively in probe-treated samples, corresponding to the expected aziridine ring-opening product (Fig. 2b). A closed search for the expected mass across nine nucleophilic residues revealed a total of 2,127 modifications, with a pronounced chemoselectivity for carboxylic acid side chains, which accounted for 68.2% of all adducts (Fig. 2c, Table S1). Interestingly, despite their high nucleophilicity,[32] cysteines represented less than 2% of the total modifications. Consensus sequence analysis further revealed that polyacidic stretches were preferentially enriched, including up to three additional Asp or Glu residues near the site of labeling (Fig. 2d).

The probe-modified proteins include well-established clinical targets as well as currently undruggable proteins, such as the highly mutated Niemann-Pick C1 protein (NPC1), implicated

in Niemann-Pick disease type C,[33] and the disulfide oxidoreductase TMX1, a potential target for immunosuppressive therapy[34] (Fig. 2e). While primarily localized to the nucleus and cytosol, the targets of **1** also span across organelles including the ER, mitochondria, and lysosome (Fig. 2f). To further evaluate the biological significance of the modified targets, we performed gene ontology (GO) analysis (Fig. 2g). Among the top ten enriched GO terms, fatty acid binding and metabolism were the most represented functions, likely due to the hydrophobicity of probe **1**.

In summary, we demonstrated that the *N*-aryl aziridine probe **1** preferentially modifies acidic residues, achieving ~70% chemoselectivity for carboxylic acids over other nucleophiles. DFT calculations suggest that this chemoselectivity arises from a reduced energy barrier facilitated by an intramolecular ring-opening mechanism involving two carboxylate groups. The probe targets diverse subcellular locations, including the nucleus, ER, mitochondria, and lysosome, and modifies previously undruggable proteins such as NPC1 and TMX1. These findings highlight the potential of *N*-aryl aziridines as a versatile scaffold for targeting the acidic proteome for covalent ligand discovery.

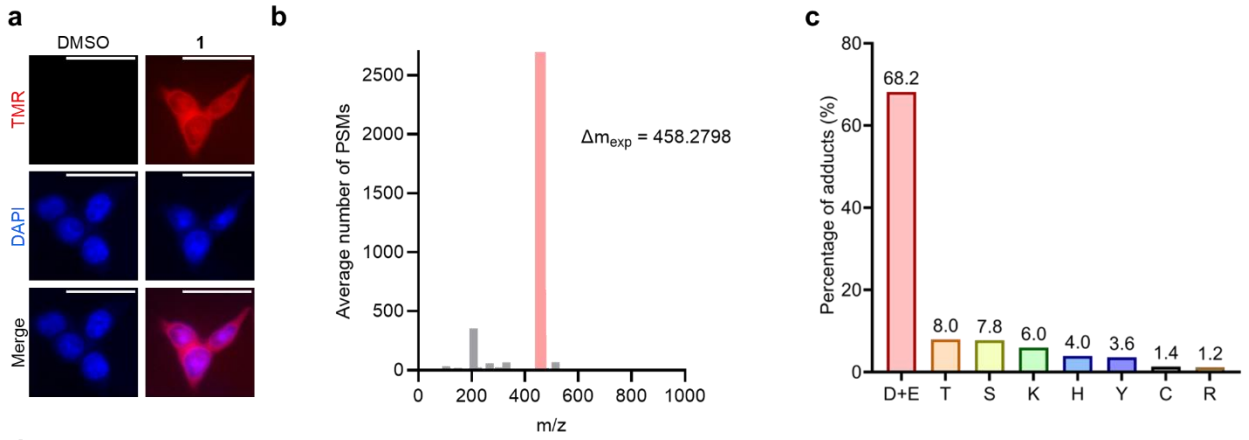

Gene Name	Protein Name	Modified Sequence
NPC1	Niemann-Pick C1 protein	VTTNPVD*LWSAPSSQAR
TMX1	Thioredoxin-related transmembrane protein 1	VD*VTEQPGLSGR
ACSL5	Long-chain-fatty-acid--CoA ligase 5	IYDKVQNE*AK
FDFT1	Squalene synthase	ALD*TLEDDMTISVEK

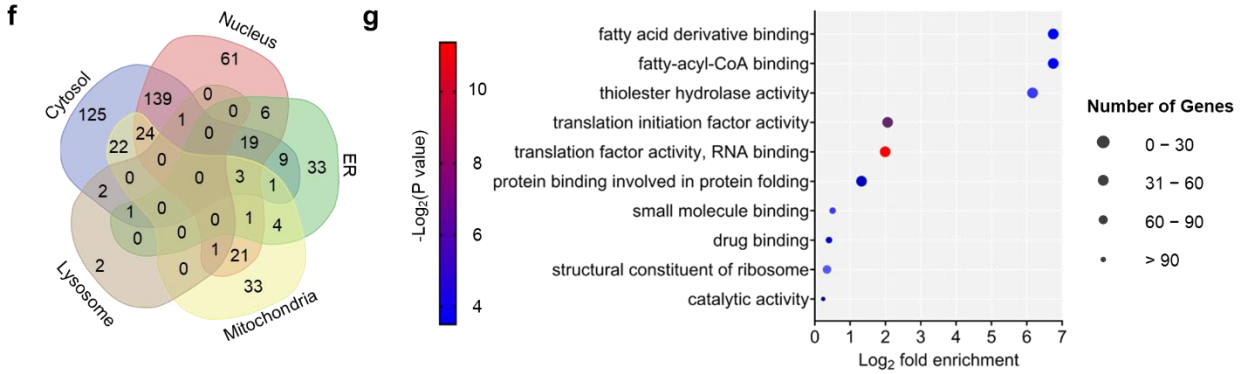

Figure 2. Disubstituted aziridine targets proteome-wide acidic residues. (a) Immunofluorescence microscopy images of HCT116 cells treated with DMSO or 100 µM probe **1** for 4 h and probe-modified proteins were conjugated to tetramethyl rhodamine (TMR) alkyne for visualization. Scale bar represents 10 µm. (b) Bar graph representing the delta masses observed in live HCT116 cells treated with probe

100 μM probe **1** for 4 h followed by site-of-labeling proteomics analysis. exp: expected. obs: observed. (c) Bar graph representing the *in situ* chemoselectivity of probe **1** (100 μM, 4 h) in HCT116 cells. (d) Logo plot of the heptameric consensus sequence of probe **1** (100 μM, 4 h) modification in HCT116 cells. (e) Table of represented clinical targets and undruggable proteins with disease relevance and their sites of modification by **1** (100 μM, 4 h) in HCT116 cells. Asterisk indicates probe modified residue. (f) Venn diagram of the subcellular distribution of **1**-modified proteins (100 μM, 4 h) in HCT116 cells. (g) Ten most enriched GO-terms among protein targets of **1** (100 μM, 4 h) in HCT116 cells.

***N*-aryl substitution of aryl aziridines confers tunable reactivity.** Having established the chemoselectivity of **1**, we next explored the tunability and proteome-wide structure-activity relationship (SAR) of aziridines by varying the *N*-aryl substituents. To achieve this, we generated a collection of differentially substituted *N*-aryl aziridine fragments via Ni-catalyzed coupling with aryl boronic acids to act as binding competitors of **1** (Fig. 3a). HCT116 cells were pretreated with unfunctionalized competitors (**2a**–**2g**, 10 μM, 4 h) and subsequently labeled with 3 μM of **1** for 1 hour. The probe concentration was optimized to prioritize hyperreactive aspartates and glutamates that exhibit significant reactivity even at lower probe concentrations. Following treatment, the cells were lysed, and probe-modified proteins were conjugated to either tetramethyl rhodamine (TMR) alkyne for in-gel fluorescence visualization or biotin alkyne for streptavidin enrichment and LC-MS/MS analysis after digestion. Notably, fragments **2a**–**2g** displayed distinct competition profiles for three primary target bands in gels (Figs. 3b, S4). Substitution at the 4-position with an electron-withdrawing ethyl ester group in fragment **2a** showed the strongest competition for two targets at approximately 40 kDa and 60 kDa, whereas *N*-tolyl aziridine **2g** exhibited minimal competition.

Subsequent LC-MS/MS proteomics analysis identified 627 probe-enriched proteins, with competition ratios calculated for each fragment (Fig. 3c, Table S2). A significant subset of these proteins (81 unique hits, ~13%) were competed ($0 < \text{ratio} \leq 0.5$) by at least one fragment. Consistent with the differential target engagement profiles, substitution at the 4-position significantly altered the protein reactivity of the core aziridine. Likely due to its electron-withdrawing properties, the ethyl ester derivative **2a** displayed the greatest number of competed targets (62), (Fig. 3d). Owing to its structural similarity to probe **1**, phenyl aziridine **2b** also exhibited considerable competition with 33 targets. Consistent with the gel-based results, *N*-tolyl aziridine **2g** demonstrated significantly reduced reactivity, competing only three targets shared with other fragments (Fig. 3d, Table S2). Principal component analysis (PCA) grouped the hits based on shared characteristics, identifying four partially overlapping clusters. These clusters reflect the shared core electrophile, suggesting a significant number of common interactions in the proteome (Fig. 3e). However, each cluster also included unique hits, underscoring the role of subtle changes in aziridine substituents in diversifying target engagement.

Lastly, we examined the subcellular distribution of high-occupancy hits (Fig. 3f). Proteins competed by fragments were predominantly localized to the endoplasmic reticulum (ER). Indeed, ER-localized proteins accounted for at least 60% of the total hits, with preferential interactions observed in other vesicular trafficking compartments, such as the Golgi apparatus, endosomes, and lysosomes.

In conclusion, these results demonstrate that *N*-substitution of aryl aziridines effectively tunes their reactivity and specificity, enabling preferential targeting of distinct protein populations.

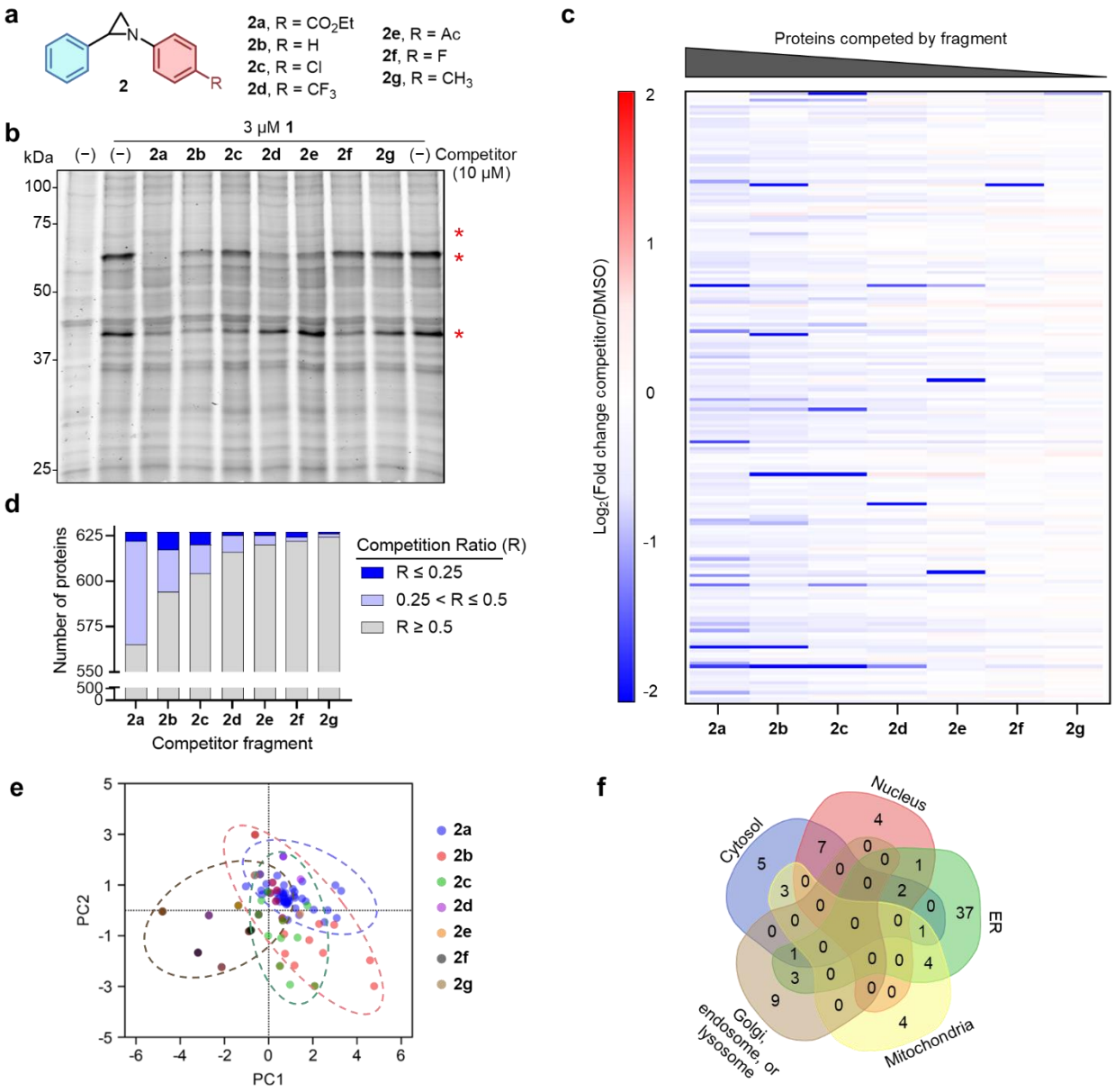

Figure 3. Disubstituted aziridines confer tunable protein reactivities through *N*-substitution. (a) Chemical structures of the competitor fragments. (b) Gel-based competitive profiling of fragments **2a**–**2g** (10 μM, 4 h) against probe **1** (3 μM, 1 h) in live HCT116 cells. Red asterisks indicate bands with significant competition. (c) Heatmap of LC-MS/MS-based *in situ* competitive profiling of fragments **2a**–**2g** (10 μM, 4 h) against probe **1** (3 μM, 1 h) in live HCT116 cells. (d) Bar graph representing the number of competed targets for each competitor fragment. (e) PCA plot of proteins competed with at least one fragment. Cumulative proportion of variance of PC1 and PC2 = 72.96%. (f) Venn diagram of the subcellular distribution of proteins competed by at least one fragment.

Proteome-wide screening of Glu and Asp targets of N-pyridinium aziridine intermediates. We sought to evaluate whether our modular synthesis of aziridines could be adapted for the rapid one-step generation of scout fragments. To this end, we synthesized a library of *N*-pyridinium aziridines (Fig. S5) to systematically identify proteome-wide ligandable Glu and Asp residues. These *N*-pyridinium aziridine scout fragments could then be optimized for specific target binding by conversion to the corresponding *N*-aryl aziridines (Fig. 1b).

Using a family of olefinic starting materials, we synthesized a 28-member library of *N*-pyridinium aziridines with an average molecular weight of 586 Da. To diversify target-binding specificity, the aryl olefin precursor was modified with electron-donating (EDG) or electron-withdrawing groups (EWG) at different positions on the aryl ring. Additionally, the library included polycyclic and alkyl pyridinium aziridines, as well as pharmaceutical derivatives and pharmacophores commonly found in bioactive natural products.

We screened the *N*-pyridinium aziridines using gel-based competitive profiling with **1** as the labeling probe. Live human colorectal carcinoma HCT116 cells were pre-incubated with each individual *N*-pyridinium aziridine fragment (10 μM, 4 h) and subsequently labeled with **1** (30 μM, 1 h). After cell lysis, the probe-labeled proteins were conjugated to TMR-alkyne for fluorescence visualization. Through fluorescence gel profiling, we identified several competed bands for each fragment (Fig. S6). Notably, variations in the substituents resulted in distinct banding patterns, reflecting the differential target landscapes of the fragments. Based on their unique competition profiles, we prioritized ten fragments for further analysis (Figs. 4a, S7, S8). These fragments were subjected to competitive LC-MS/MS-based chemoproteomics to identify their proteome-wide aspartate and glutamate targets.

Following sequential treatment with the competitor (10 μM, 4 h) and **1** *in situ* (30 μM, 1 h), HCT116 cells were lysed, and the probe-modified proteins were conjugated to desthiobiotin alkyne. The proteins were then digested into tryptic peptides, enriched using streptavidin, and analyzed by LC-MS/MS (Fig. 4b). Among the 1,673 probe-modified Glu or Asp residues, ligandable sites were identified by applying a non-zero competition ratio threshold of ≤ 0.3 relative to the DMSO control (Fig. 4c, Table S3). Overall, approximately 16% (≥ 250) of the probe-modified residues were significantly liganded by one or more *N*-pyridinium aziridine fragments, a level comparable to ligandability parameters observed for reactive cysteines and tyrosines.[14, 35]

The competed hits included several previously undruggable proteins, similar to those identified in probe-enrichment studies alone (Fig. 2f). Notably, the putative mitochondrial insertase, mitochondrial carrier homolog 2 (MTCH2), contained a hotspot residue (D118, Fig. S9) that was selectively targeted by several fragments with varying affinities. The three highest-affinity hits, **3a**–**c**, featured either unsubstituted or *para*-functionalized phenyl substituents, whereas *ortho*- and *meta*-substituted phenyl groups competed the MTCH2 labeling significantly less (Fig. 4d). MTCH2 plays a critical role in mitochondrial alpha-helical protein transport and acts as a gatekeeper for mitochondrial outer membrane biogenesis.[36] It has been challenging to target due to its membrane-embedded hydrophobic core. Liganding MTCH2 via *N*-substituted aziridines may therefore represent a promising strategy for targeting this protein.

Another example of an undruggable protein is the endosomal scaffold RUN and FYVE domain-containing protein 1 (RUFY1), which participates in cargo sorting from early endosomes to recycling endosomes.[37] Our analysis indicates that E502 (Fig. S10) is liganded by four different fragments, with *ortho*-substituted **3h** and **3i** demonstrating the highest occupancy. Interestingly, fragment **3j** also exhibited significant competition and showed remarkable proteome-wide selectivity in both gel- and LC-MS/MS-based profiling (Figs. 4d, S6, S8). In the gel-based profiling, a single competed band was observed (Figs. S6, S8), while LC-MS/MS analysis identified a total of 14 hit residues across 10 proteins, including RUFY1 E502 and delta(24)-sterol reductase (DHCR24) D436 (Fig. S11, Table S3).

In summary, our findings demonstrate that substituted *N*-pyridinium aziridine fragments effectively engage previously untargetable proteins through covalent modification of acidic residues.

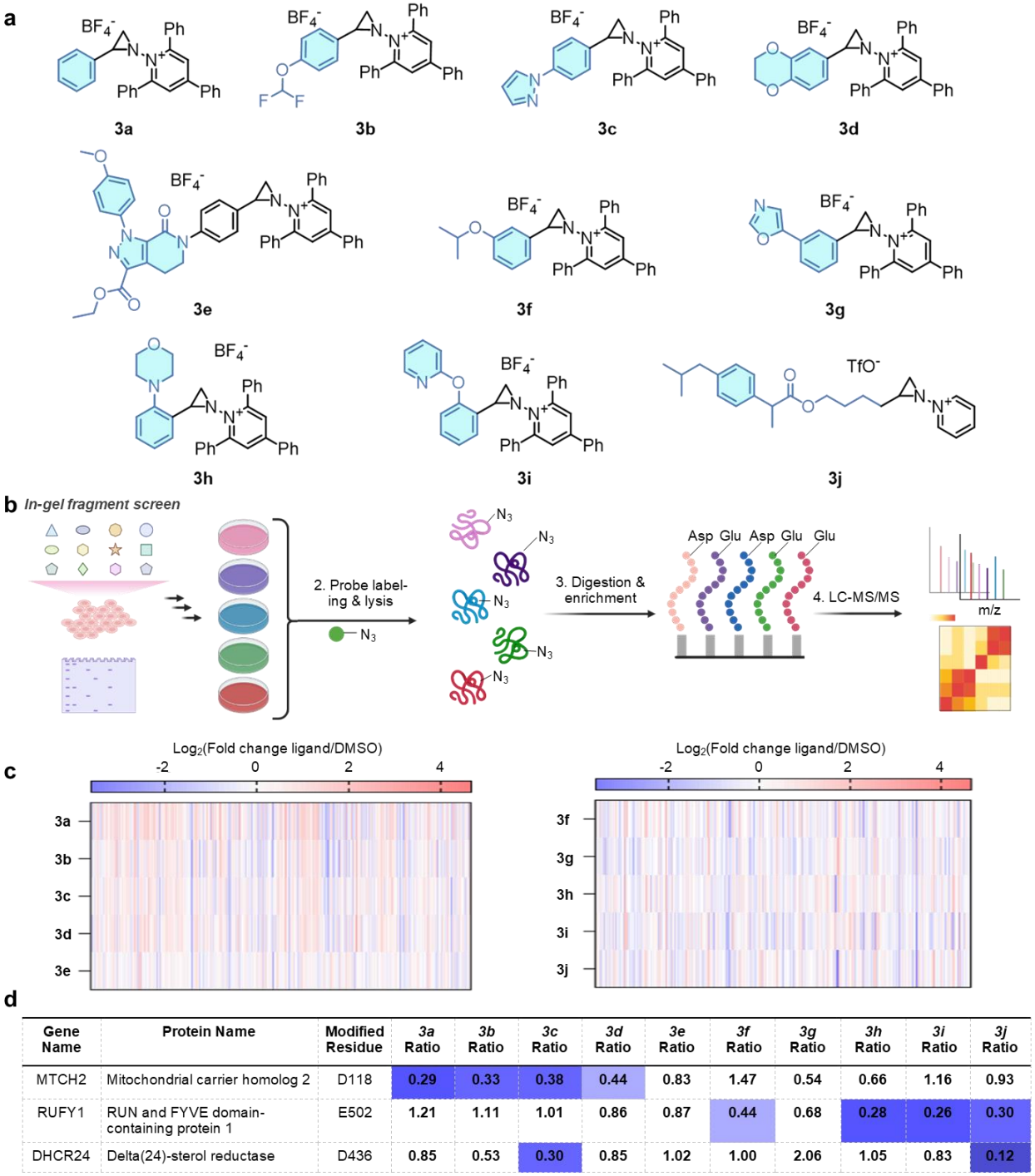

d

Gene Name	Protein Name	Modified Residue	*3a* Ratio	*3b* Ratio	*3c* Ratio	*3d* Ratio	*3e* Ratio	*3f* Ratio	*3g* Ratio	*3h* Ratio	*3i* Ratio	*3j* Ratio
MTCH2	Mitochondrial carrier homolog 2	D118	**0.29**	**0.33**	**0.38**	**0.44**	**0.83**	**1.47**	**0.54**	**0.66**	**1.16**	**0.93**
RUFY1	RUN and FYVE domain-containing protein 1	E502	**1.21**	**1.11**	**1.01**	**0.86**	**0.87**	**0.44**	**0.68**	**0.28**	**0.26**	**0.30**
DHCR24	Delta(24)-sterol reductase	D436	**0.85**	**0.53**	**0.30**	**0.85**	**1.02**	**1.00**	**2.06**	**1.05**	**0.83**	**0.12**

Figure 4. Proteome-wide profiling of Glu and Asp targets of *N*-pyridinium aziridine fragments. (a). Chemical structures of selected *N*-pyridinium aziridine fragments **3a**–**3j** used in the LC-MS/MS-based target screening assay. (b) Schematic representation of competitive reactive Glu and Asp profiling using in-gel visualization and competitive site-of-labeling enrichment proteomics. (c) Heatmap representation of LC-MS/MS-based target screening of selected pyridinium aziridine fragments **3a**–**3j**. (d) Table of three represented probe-modified acidic residues on target proteins and their competition ratios by corresponding *N*-pyridinium aziridine fragments **3a**–**3j**.

Fragment evolution yields N-aryl aziridines to ligand acidic residues. We first proceeded to validate the chemoproteomics results on MTCH2, RUFY1, and DHCR24 via chemical pulldowns.

To prioritize fragments for serial variation of the exocyclic nitrogen valence via C–N cross-coupling, we selected *N*-pyridinium aziridine **3a** for its low competition ratio in targeting MTCH2 and fragment **3j** for its high occupancy binding to RUFY1 and DHCR24 and remarkable proteome-wide selectivity. HEK293T cells overexpressing FLAG-tagged target proteins were preincubated with the corresponding fragment (10 µM, 4 h), followed by probe labeling (30 µM, 1 h). After lysis, the probe-labeled proteins were conjugated to biotin-alkyne for enrichment via streptavidin prior to immunoblotting.

We consistently observed that the ligands competed with probe labeling of all three targets in a concentration-dependent manner (Fig. 5a), indicating that the *N*-pyridinium aziridines bind to the same site as probe **1**. Site-directed mutagenesis of the probe-modified aspartate and glutamate residues significantly reduced probe binding, confirming these residues as the primary interaction sites (Fig. 5b). Notably, among the three targets, fragment **3j** demonstrated nearly complete competition with DHCR24 labeling at a concentration of 10 µM. This particular example highlights the feasibility of identifying potent and selective *N*-pyridinium aziridine fragments without requiring further optimization through second-step derivatization.

To demonstrate how our hit fragments can be fine-tuned by variation of the exocyclic nitrogen valence, **3a** was converted into corresponding *N*-aryl aziridines via Ni-catalyzed cross-coupling with various arylboronic acids, and their binding affinities to overexpressed FLAG-MTCH2 (F-MTCH2) were assessed using chemical pulldown (Fig. 5c). Unexpectedly, substitutions with highly electron-withdrawing groups, such as cyano, 3,5-bis(trifluoromethyl), and nitro groups, abolished the interaction with MTCH2 instead of improving competition by enhancing the reactivity of the aziridine ring (Fig. 5d). Conversely, the phenyl-substituted fragment **4b** exhibited the strongest competition among the aryl aziridines and modestly outperformed the original *N*-pyridinium aziridine **3a**. These findings suggest that the increased affinity of **4b** for F-MTCH2 may be attributed to additional non-covalent interactions rather than solely to the intrinsic electrophilicity of the warhead.

As a second example of fine-tuning a scout fragment by transforming it into *N*-aryl aziridine ligands, we synthesized compounds **5a**–**e** from fragment **3j** (Fig. 5e) and evaluated their binding to overexpressed RUFY1-FLAG (RUFY1-F). Similar to the MTCH2 ligands, several **3j**-derived *N*-aryl aziridines retained the ability to bind RUFY1-F, with the methyl-ester-substituted ligand **5b** demonstrating the strongest competition (Fig. 5f). Notably, **5b** exhibited superior affinity compared to the original intermediate **3j**, as shown by a more than twofold improvement in competition. Substitution of the *para*-position with an electron-withdrawing nitro group abolished binding, underscoring the combined importance of molecular recognition and reactivity for effective target engagement.

When comparing the relative occupancies of the ligands, we found that methyl ester derivatives generally maintained high affinities, whereas strongly electron-withdrawing groups such as cyano and nitro substituents hindered binding (Figs. 5d, 5f). Taken together, our results demonstrate that generating *N*-aryl aziridine ligands from *N*-pyridinium intermediates is a viable strategy for accessing carboxylate-directed ligands targeting previously undruggable proteins.

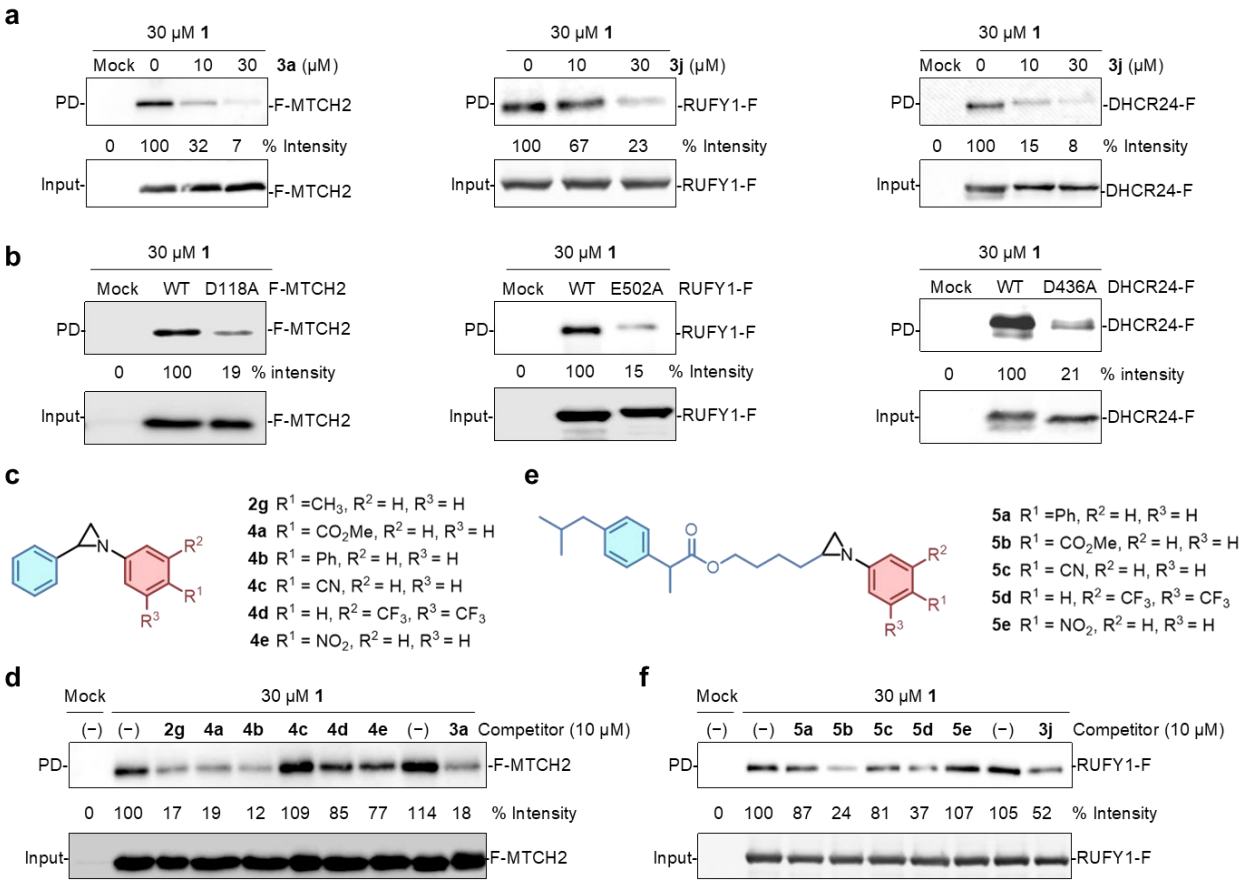

Figure 5. Fragment evolution yields *N*-aryl aziridines to ligand acidic residues. (a) Immunoblotting of *in situ* competitive chemical pulldown experiment of hit ligands with probe **1** in HEK293T cells overexpressing F-MTCH2 (left), RUFY1-F (middle), or DHCR24-F (right). (b) Immunoblotting of *in situ* chemical pulldown with probe **1** in HEK293T cells overexpressing WT or corresponding D/E mutants of F-MTCH2 (left), RUFY1-F (middle), or DHCR24-F (right). (c) Chemical structures of *N*-aryl aziridines derived from **3a** to target MTCH2. (d) Competitive chemical pulldown of *N*-aryl aziridines against probe **1** in live HEK293T cells overexpressing F-MTCH2. (e) Chemical structures of *N*-aryl aziridines derived from **3j** to target RUFY1. (f) Competitive chemical pulldown of *N*-aryl aziridines against probe **1** in live HEK293T cells overexpressing RUFY1-F.

Targeting an on-catalytic glutamic acid in RUFY1 disrupts endosomal recycling. To investigate the functional impact of targeting acidic residues with *N*-aryl aziridines, we focused on the human RUFY1 protein due to its non-enzymatic scaffolding role in endosomal recycling, which presents a significant challenge for the design of traditional inhibitors. Loss of RUFY1 disrupts the recycling of endocytosed transferrin receptor and epidermal growth factor receptors (EGFR), leading to their retention in early endosomes.[37-40] Structurally, RUFY1 is predicted to adopt a long, tubular shape with two folded terminal domains, acting as a bridge between phosphatidylinositol 3-phosphate (PI3P)-enriched vesicles and small GTPases on the microtubule (Fig. 6a).[41] Truncation of its coiled-coil regions mislocalizes RUFY1 and abolishes its co-localization with the early endosomal marker EEA1.[42] Notably, the probe-modified glutamic acid residue, E502, is located within the second non-catalytic coiled-coil region, which mediates protein-protein interactions.[41] Based on these findings, we sought to determine whether targeting E502 with *N*-aryl aziridines could inhibit the activity of this otherwise undruggable protein.

We first performed a transferrin (Tfn) recycling assay,[38] utilizing a fluorescent Tfn conjugate (Figs. 6b–c, S12). Briefly, HeLa cells were deprived of transferrin for 4 hours before

pulse labeling with Tfn-488 (50 µg/mL, 5 min). Surface-bound Tfn-488 was removed by acid wash, and cells were subsequently chased with unlabeled transferrin (500 µg/mL) for indicated amount of time. Strikingly, treatment with the active *N*-aryl aziridine **5b** (10 µM) rapidly retained Tfn-488 in the perinuclear space within 4 hours, mimicking the effect observed in RUFY1 knockdown (KD) cells transfected with siRNA for 72 hours. In contrast, treatment with the inactive control compound **5e** had no impact on recycling kinetics, suggesting that **5b** acts via a RUFY1-dependent mechanism.

Similarly, we observed a rapid inhibition of EGFR recycling using fluorescently labeled EGF in A431 cells, where high EGFR expression is often exploited to study this signaling pathway. Treatment with **5b** or RUFY1 siRNA resulted in prolonged retention of EGF-647, co-localized with the early endosomal marker EEA1 but not the lysosomal marker LAMP1, at both 30-minute and 60-minute time points (Figs. 6d–e, S13). This observation indicated defects in endosome recycling and maturation to fuse with lysosome. Importantly, the total protein level of EGFR remained unaffected (Fig. S14). We hypothesized that defective recycling might alter the subcellular distribution of EGFR, favoring its retention in early endosomes over its presence on the cell surface. To test this hypothesis, we co-stained EGFR with EGF-647 in A431 cells in the recycling assay and quantified intracellular EGF–EGFR puncta (Figs. 6f, S15). As expected, treatment with **5b** or RUFY1 knockdown resulted in prolonged EGF–EGFR retention in intracellular compartments. Cells with increased intracellular puncta also exhibited significantly decreased EGFR signal at the cell surface, confirming that RUFY1 inhibition redirects the receptor to endomembrane compartments instead of the plasma membrane. To evaluate the effect of RUFY1 inhibition on EGFR signaling, we measured the phosphorylation of ERK kinase, a downstream effector of EGFR activation (Fig. 6g). As expected, given that EGFR remains active within endosomes, treatment with **5b** or RUFY1 siRNA resulted in sustained ERK phosphorylation over 60 minutes. This indicates that despite defective RUFY1-mediated trafficking, EGFR signaling persists from intracellular compartments with increased signaling duration. Collectively, our findings underscore the critical role of RUFY1 in regulating the spatial dynamics of EGFR signaling by facilitating receptor recycling and subcellular localization.

Finally, we sought to determine whether **5b** potentially disrupts interactions between RUFY1 and its binding partners. To this end, we performed co-immunoprecipitation proteomics in HEK293T cells expressing RUFY1-F, with or without **5b** treatment (10 µM, 4 h). Protein interactors were identified using LC-MS/MS (Fig. 6h, Table S4). We focused on changes in proteins involved in vesicular trafficking and proteostasis, as these pathways are intricately linked to endosomal recycling. As expected, known RUFY1-F interactors,[38] such as the small GTPases Rab14 and Rab21, were effectively enriched, with Rab14 displaying a moderate decrease in RUFY1 binding upon **5b** treatment. More intriguingly, we identified ALG-2 interacting protein X (Alix, encoded by the PDCD6IP gene), a critical mediator of fluid-phase endocytosis and multivesicular body biogenesis,[43, 44] as a novel interactor of RUFY1-F. Treatment with **5b** disrupted the interaction between RUFY1-F and Alix in a concentration-dependent manner (Fig. 6i), indicating that liganding RUFY1 E502 impairs its scaffolding function (Fig. 6j).

In summary, our findings demonstrate that site-specific pharmacological targeting of RUFY1 at residue E502 offers a powerful approach to selectively modulate its role in endosomal trafficking and receptor recycling processes. By disrupting specific protein-protein interactions, such as those with Alix, we revealed critical mechanistic insights into how RUFY1 regulates endosomal recycling, maturation, and proteostasis pathways. This strategy not only enables a deeper understanding of the molecular functions of RUFY1 but also provides a valuable tool for probing the broader implications of endosomal dysfunction in cellular signaling and disease states.

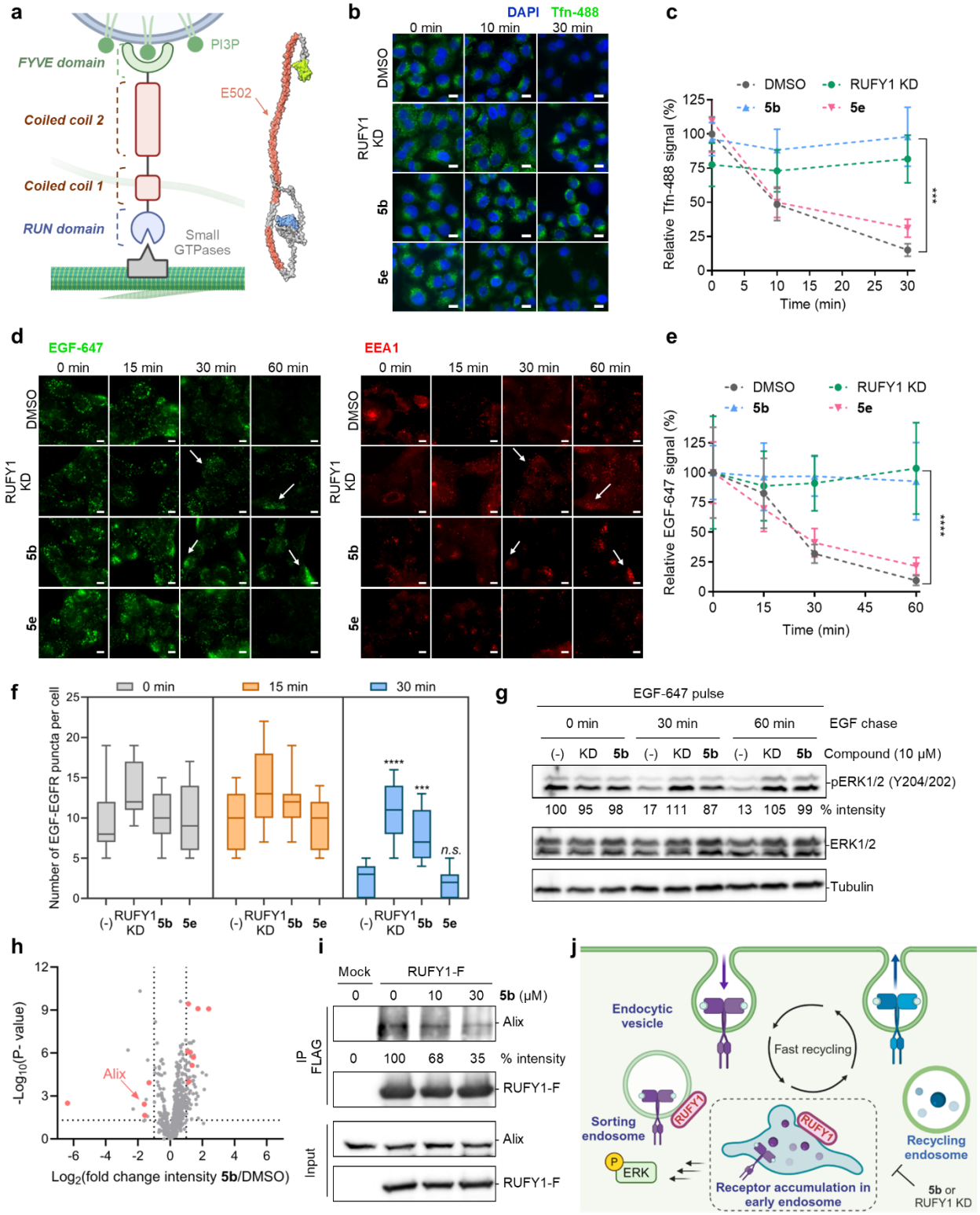

Figure 6. Targeting a non-catalytic glutamic acid residue in RUFY1 disrupts endosome-mediated receptor recycling. (a) Domain organization and AlphaFold-predicted structure of RUFY1 that mediates binding to PIP3-rich vesicles and small GTPases. (b) Fluorescence microscopy images and (c) thereof quantifications of transferrin recycling assay in HeLa cells treated with **5b** or **5e** (10 μM, 4h) or RUFY1 siRNA (72 h). The cells were pulsed for 5 min with 50 μg/mL Tfn- Alexa 488 and then chased with 500 μg/mL Tfn for indicated

amount of time. KD, knockdown. (d) Fluorescence microscopy images and (e) thereof quantifications of EGFR recycling assay in A431 cells treated with **5b** or **5e** (10 µM, 4h) or RUFY1 siRNA (72 h) and co-stained with EEA1 and LAMP1. The cells were pulsed with 30 min of 20 ng/mL EGF-Alexa 647 and then chased with 200 ng/mL EGF for indicated amount of time. (f) Boxplot measuring the number of EGFR puncta co-localized with EGF-Alexa 647 in A431 cells treated with **5b** or **5e** (10 µM, 4h) or RUFY1 siRNA (72 h) and co-stained with EGFR. (g) Immunoblotting of ERK phosphorylation in A431 cells treated with **5b** (10 µM, 4h) or RUFY1 siRNA (72 h). The cells were pulsed with 30 min of 20 ng/mL EGF-Alexa 647 and then chased with 200 ng/mL EGF for indicated amount of time. (h) Volcano plot of co-immunoprecipitation proteomics in HEK293T cells overexpressing RUFY1-F and treated with DMSO or **5b** (10 µM, 4h). Pink dots denote proteins in proteostasis or vesicular trafficking with significant changes upon **5b** treatment. (i) Co-immunoprecipitation of RUFY1-F in HEK293T cells and western blotting of ALIX upon *in situ* treatment of **5b** for 4 h. (j) Schematic representation of RUFY1 inhibition leading to disrupted endosome-mediated receptor recycling. *** indicates $p < 0.001$ and **** indicates $p < 0.0001$ in two-way ANOVA test. $n \geqslant 10$. Scale bar represents 10 µm.

Discussion

In summary, we introduced *N*-aryl aziridines as a versatile scaffold for proteome-wide covalent targeting of acidic residues, employing a modular *build-and-couple* strategy for rapid ligand elaboration. Using an *N*-aryl aziridine-based chemical probe, we profiled over 2,000 acidic residues in live cells, uncovering a particular chemoselectivity of *N*-aryl aziridines for aspartic and glutamic acids for the first time. We synthesized and screened a diverse library of *N*-pyridinium aziridine intermediates and identified ligands for previously undruggable proteins such as MTCH2 and RUFY1. Transforming the *N*-pyridinium aziridine fragment **3j** into *N*-aryl aziridine **5b** enhanced RUFY1 binding affinities, highlighting the unique advantages of fragment evolution through second-step diversification. Furthermore, we demonstrated that site-specific targeting of a non-catalytic glutamate residue (E502) disrupts RUFY1's scaffolding function and impairs endosomal recycling of cell surface receptors. Co-immunoprecipitation proteomics revealed that treatment with **5b** alters the RUFY1 interactome, particularly reducing its binding to Alix, a key mediator of endosome sorting. Collectively, our study not only underscores the therapeutic potential of covalently targeting non-catalytic aspartates and glutamates but also offers a robust synthetic strategy for designing and rapidly generating aziridine-based protein ligands.

Pinpointing acidic residues offers several advantages for expanding the ligandable proteome. The combined abundance of aspartic and glutamic acids in proteins represents ~12% of all amino acids, outnumbering the commonly targeted cysteine residues (~1%) by more than 10-fold.[45] Although active-site aspartic proteases can be potently inhibited by transition state analogs and substrate-based inhibitors,[7, 24] non-catalytic carboxylic acids represent an exciting opportunity for covalent targeting, as these residues harbor unique reactivity hotspots akin to those of other reactive amino acids.[11, 35, 46-48] Indeed, our scrutiny of the acidic proteome revealed a subset of polyacidic stretches susceptible to aziridine modification. The competitive profiling of **2a**–**g** subsequently revealed that the high-occupancy binders are enriched in endomembrane compartments, illuminating the potential to influence key cellular processes such as protein folding and vesicular trafficking, as we subsequently demonstrated with the RUFY1 inhibitor **5b**. To access a wider range of carboxylic acids, advanced fractionation techniques can be incorporated in the future for deeper profiling across the subcellular environment. Additional tuning of the aziridine ring could also yield chemical probes that modify a broader and/or distinct subset of acidic residues without compromising the chemoselectivity.

Our study highlights aziridines as a versatile scaffold for covalent inhibitor design and drug discovery. Unlike naturally occurring polycyclic aziridines, which are often potent DNA-alkylating agents,[30] we demonstrate that *N*-aryl aziridines selectively modify proteins without inducing DNA damage in cells. This differential reactivity of the aziridine electrophile between DNA and proteins is crucial for minimizing off-target effects and enhancing their safety profile for therapeutic

applications. The small molecular size of the electrophile (probe **1** is 249 Da) supports its application in a ligand-first approach for covalent inhibitor development, where low-affinity, non-covalent fragments can be functionalized with the aziridine warhead to enhance potency and expand the range of accessible targets. Our modular synthesis of *N*-aryl aziridines via *N*-pyridinium aziridine intermediates offers several unique advantages. Sequential olefin *N*-aminopyridylation and cross-coupling reactions enable diversification of both nitrogen and carbon substituents, accommodating a wide range of drug-like substrates with high sp^3 content in our fragment library. Furthermore, the intermediary pyridinium aziridine fragments themselves can exhibit unique reactivity toward acidic residues, as demonstrated by the potent competition of DHCR24 D436 by **3j**. In the future, synthesizing and systematically evaluating additional moderately electrophilic, non-aryl aziridines may provide valuable opportunities to engage protein targets that are inaccessible to *N*-aryl aziridines.

Finally, our discovery of a first-in-class small-molecule RUFY1 inhibitor marks a significant advancement in understanding its role in vesicular trafficking. We demonstrated that **5b** enables rapid RUFY1 inhibition within just 4 hours, effectively phenocopying the effects of genetic knockdown achieved over three days. This provides a valuable tool for investigating RUFY1-mediated protein transport mechanisms. For instance, our co-immunoprecipitation proteomics revealed that **5b** reduces the interaction between RUFY1 and its endosomal sorting partner, Alix.[43, 44] Additionally, RUFY1 inhibitors can help identify recycling receptors involved in RUFY1-dependent sorting. Deconstructing these sorting mechanisms may unlock new opportunities for selectively manipulating subsets of recycling receptors for basic research or therapeutic purposes. For example, the endosomal recycling pathway is often exploited by pathogens to facilitate infection and replication within host cells. Notably, RUFY1 is recruited to early endosomes containing the intracellular periodontal pathogen *Porphyromonas gingivalis*, aiding the pathogen's exit and evasion of lysosomal destruction.[49] Other pathogens, such as *Salmonella enterica* and *Mycobacterium tuberculosis*,[50-52] also exploit early endosomal compartments for survival and replication, highlighting the critical role of endosomal trafficking in host-pathogen interaction. Therefore, inhibiting RUFY1 presents a potential strategy to mitigate infection and synergize with broad-spectrum antibacterials. In this context, RUFY1 inhibitors not only provide a powerful tool for advancing the fundamental understanding of vesicular trafficking but also open new avenues for therapeutic interventions targeting host-pathogen interactions and cellular transport.

ASSOCIATED CONTENT

Supporting Information

The supporting Information is available free of charge at

Complete experimental details and procedures, supporting figures, and NMR spectra.

Mass spectrometry proteomics data

AUTHOR INFORMATION

Corresponding Author

aadibeki@uic.edu, powers@chem.tamu.edu

ORCID

Alexander Adibekian: 0000-0001-6453-0244

David C. Powers: 0000-0003-3717-2001

Notes

Preliminary results of this study have been disclosed in a pair of provisional patent filings with A.A., D.C.P., H.T., and N.Q. as inventors.

ACKNOWLEDGMENT

This work was supported by the National Institutes of Health grants RO1GM145886 (to A.A.) and R35GM138114 (to D.C.P.), and Enveda Biosciences sponsored research grant (to A.A.), UIC LAS Endowed Professorship (to A.A.), and the Welch Foundation grant A-1907 (to D.C.P.). N.Q. was supported by the NSF Graduate Research Fellowships Program and Reba and Nat Endowed Fellowship, and the Scripps Research Institute.

References

(1) Flotow, H.; Roach, P. J. Role of Acidic Residues as Substrate Determinants for Casein Kinase-I. *Journal of Biological Chemistry* **1991**, *266* (6), 3724-3727.
(2) Pace, N. J.; Weerapana, E. Zinc-binding cysteines: diverse functions and structural motifs. *Biomolecules* **2014**, *4* (2), 419-434. DOI: 10.3390/biom4020419 From NLM Medline.
(3) Dean, J. L. E.; Wang, X. G.; Teller, J. K.; Waugh, M. L.; Britton, K. L.; Baker, P. J.; Stillman, T. J.; Martin, S. R.; Rice, D. W.; Engel, P. C. The Catalytic Role of Aspartate in the Active-Site of Glutamate-Dehydrogenase. *Biochem J* **1994**, *301*, 13-16. DOI: DOI 10.1042/bj3010013.
(4) Xuan, W.; Ma, J. A. Pinpointing Acidic Residues in Proteins. *ChemMedChem* **2024**, *19* (5), e202300623. DOI: 10.1002/cmdc.202300623 From NLM Medline.
(5) Eder, J.; Hommel, U.; Cumin, F.; Martoglio, B.; Gerhartz, B. Aspartic proteases in drug discovery. *Curr Pharm Design* **2007**, *13* (3), 271-285. DOI: Doi 10.2174/138161207779313560.
(6) Turner, S. R.; Strohbach, J. W.; Tommasi, R. A.; Aristoff, P. A.; Johnson, P. D.; Skulnick, H. I.; Dolak, L. A.; Seest, E. P.; Tomich, P. K.; Bohanan, M. J.; et al. Tipranavir (PNU-140690): A potent, orally bioavailable nonpeptidic HIV protease inhibitor of the 5,6-dihydro-4-hydroxy-2-pyrone sulfonamide class. *J Med Chem* **1998**, *41* (18), 3467-3476. DOI: DOI 10.1021/jm9802158.
(7) Ghosh, A. K.; Dawson, Z. L.; Mitsuya, H. Darunavir, a conceptually new HIV-1 protease inhibitor for the treatment of drug-resistant HIV. *Bioorgan Med Chem* **2007**, *15* (24), 7576-7580. DOI: 10.1016/j.bmc.2007.09.010.
(8) Weerapana, E.; Wang, C.; Simon, G. M.; Richter, F.; Khare, S.; Dillon, M. B. D.; Bachovchin, D. A.; Mowen, K.; Baker, D.; Cravatt, B. F. Quantitative reactivity profiling predicts functional cysteines in proteomes. *Abstr Pap Am Chem S* **2011**, *241*.
(9) Abegg, D.; Frei, R.; Cerato, L.; Prasad Hari, D.; Wang, C.; Waser, J.; Adibekian, A. Proteome-Wide Profiling of Targets of Cysteine reactive Small Molecules by Using Ethynyl Benziodoxolone Reagents. *Angew Chem Int Ed Engl* **2015**, *54* (37), 10852-10857. DOI: 10.1002/anie.201505641 From NLM Medline.
(10) Abegg, D.; Tomanik, M.; Qiu, N.; Pechalrieu, D.; Shuster, A.; Commare, B.; Togni, A.; Herzon, S. B.; Adibekian, A. Chemoproteomic Profiling by Cysteine Fluoroalkylation Reveals Myrocin G as an Inhibitor of the Nonhomologous End Joining DNA Repair Pathway. *J Am Chem Soc* **2021**, *143* (48), 20332-20342. DOI: 10.1021/jacs.1c09724.
(11) Hacker, S. M.; Backus, K. M.; Lazear, M. R.; Forli, S.; Correia, B. E.; Cravatt, B. F. Global profiling of lysine reactivity and ligandability in the human proteome. *Nat Chem* **2017**, *9* (12), 1181-1190. DOI: 10.1038/Nchem.2826.
(12) Abbasov, M. E.; Kavanagh, M. E.; Ichu, T. A.; Lazear, M. R.; Tao, Y. F.; Crowley, V. M.; Ende, C. W. A.; Hacker, S. M.; Ho, J. R.; Dix, M. M.; et al. A proteome-wide atlas of lysine-reactive chemistry (Sept, 10.1038/s41557-021-00765-4, 2021). *Nat Chem* **2021**, *13* (11), 1151-1151. DOI: 10.1038/s41557-021-00823-x.
(13) Hahm, H. S.; Toroitich, E. K.; Borne, A. L.; Brulet, J. W.; Libby, A. H.; Yuan, K.; Ware, T. B.; McCloud, R. L.; Ciancone, A. M.; Hsu, K. L. Global targeting of functional tyrosines using sulfur-

triazole exchange chemistry. *Nat Chem Biol* **2020**, *16* (2), 150-+. DOI: 10.1038/s41589-019-0404-5.
(14) Brulet, J. W.; Borne, A. L.; Yuan, K.; Libby, A. H.; Hsu, K. L. Liganding Functional Tyrosine Sites on Proteins Using Sulfur-Triazole Exchange Chemistry. *J Am Chem Soc* **2020**, *142* (18), 8270-8280. DOI: 10.1021/jacs.0c00648 From NLM Medline.
(15) Ma, N.; Hu, J.; Zhang, Z. M.; Liu, W. Y.; Huang, M. H.; Fan, Y. L.; Yin, X. F.; Wang, J. G.; Ding, K.; Ye, W. C.; et al. 2
-Azirine-Based Reagents for Chemoselective Bioconjugation at Carboxyl Residues Inside Live Cells. *J Am Chem Soc* **2020**, *142* (13), 6051-6059. DOI: 10.1021/jacs.9b12116.
(16) Bach, K.; Beerkens, B. L. H.; Zanon, P. R. A.; Hacker, S. M. Light-Activatable, 2,5-Disubstituted Tetrazoles for the Proteome-wide Profiling of Aspartates and Glutamates in Living Bacteria. *Acs Central Sci* **2020**, *6* (4), 546-554. DOI: 10.1021/acscentsci.9b01268.
(17) Qian, Y.; Schurmann, M.; Janning, P.; Hedberg, C.; Waldmann, H. Activity-Based Proteome Profiling Probes Based on Woodward's Reagent K with Distinct Target Selectivity. *Angew Chem Int Ed Engl* **2016**, *55* (27), 7766-7771. DOI: 10.1002/anie.201602666 From NLM Medline.
(18) Hillebrand, L.; Liang, X. J.; Serafim, R. A. M.; Gehringer, M. Emerging and Re-emerging Warheads for Targeted Covalent Inhibitors: An Update. *J Med Chem* **2024**, *67* (10), 7668-7758. DOI: 10.1021/acs.jmedchem.3c01825.
(19) Dank, C.; Ielo, L. Recent advances in the accessibility, synthetic utility, and biological applications of aziridines. *Org Biomol Chem* **2023**, *21* (22), 4553-4573. DOI: 10.1039/d3ob00424d.
(20) Degel, B.; Staib, P.; Rohrer, S.; Scheiber, J.; Martina, E.; Buchold, C.; Baumann, K.; Morschhauser, J.; Schirmeister, T. Cis-Configured aziridines are new pseudo-irreversible dual-mode inhibitors of Candida albicans secreted aspartic protease 2. *ChemMedChem* **2008**, *3* (2), 302-315. DOI: 10.1002/cmdc.200700101 From NLM Medline.
(21) Dequina, H. J.; Jones, C. L.; Schomaker, J. M. Recent updates and future perspectives in aziridine synthesis and reactivity. *Chem* **2023**, *9* (7), 1658-1701. DOI: 10.1016/j.chempr.2023.04.010 From NLM PubMed-not-MEDLINE.
(22) Zhang, J. P.; Wang, X.; Huang, Q. J.; Ye, J. S.; Wang, J. Genetically Encoded Epoxide Warhead for Precise and Versatile Covalent Targeting of Proteins. *J Am Chem Soc* **2024**, *146* (23), 16173-16183. DOI: 10.1021/jacs.4c03974.
(23) Lin, S.; Yang, X.; Jia, S.; Weeks, A. M.; Hornsby, M.; Lee, P. S.; Nichiporuk, R. V.; Iavarone, A. T.; Wells, J. A.; Toste, F. D.; et al. Redox-based reagents for chemoselective methionine bioconjugation. *Science* **2017**, *355* (6325), 597-602. DOI: 10.1126/science.aal3316 From NLM Medline.
(24) Nakata, M.; Chong, C.; Niwata, Y.; Toshima, K.; Tatsuta, K. A Family of Cyclophellitol Analogs - Synthesis and Evaluation. *J Antibiot* **1993**, *46* (12), 1919-1922. DOI: DOI 10.7164/antibiotics.46.1919.
(25) Wu, L.; Jiang, J.; Jin, Y.; Kallemeijn, W. W.; Kuo, C. L.; Artola, M.; Dai, W.; van Elk, C.; van Eijk, M.; van der Marel, G. A.; et al. Activity-based probes for functional interrogation of retaining beta-glucuronidases. *Nat Chem Biol* **2017**, *13* (8), 867-873. DOI: 10.1038/nchembio.2395 From NLM Medline.
(26) Jiang, J. B.; Kuo, C. L.; Wu, L.; Franke, C.; Kallemeijn, W. W.; Florea, B. I.; van Meel, E.; van der Marel, G. A.; Codée, J. D. C.; Boot, R. G.; et al. Detection of Active Mammalian GH31 α-Glucosidases in Health and Disease Using In-Class, Broad-Spectrum Activity-Based Probes (vol 2, pg 351, 2016). *Acs Central Sci* **2017**, *3* (6), 673-673. DOI: 10.1021/acscentsci.7b00185.
(27) Jiang, L. Y.; Menard, M.; Weller, C.; Wang, Z. C.; Burnett, L.; Aronchik, I.; Steele, S.; Flagella, M.; Zhao, R. P.; Evans, J. W. W.; et al. RMC-9805, a first-in-class, mutant-selective, covalent and oral KRAS
(ON) inhibitor that induces apoptosis and drives tumor regression in preclinical models of KRAS cancers. *Cancer Res* **2023**, *83* (7). DOI: 10.1158/1538-7445.Am2023-526.

(28) Tan, H.; Samanta, S.; Maity, A.; Roychowdhury, P.; Powers, D. C. Aminopyridinium reagents as traceless activating groups in the synthesis of
-Aryl aziridines. *Nat Commun* **2022**, *13* (1). DOI: ARTN 3341
10.1038/s41467-022-31032-w.
(29) Tan, H.; Thai, P.; Sengupta, U.; Deavenport, I. R.; Kucifer, C. M.; Powers, D. C. Metal-Free Aziridination of Unactivated Olefins via Transient
-Pyridinium Iminoiodinanes. *Jacs Au* **2024**. DOI: 10.1021/jacsau.4c00556.
(30) Maurer, S. J.; de Albuquerque, J. L. P.; McCallum, M. E. Recent Developments in the Biosynthesis of Aziridines. *Chembiochem* **2024**, *25* (16). DOI: ARTN e202400295
10.1002/cbic.202400295.
(31) Yu, F.; Haynes, S. E.; Teo, G. C.; Avtonomov, D. M.; Polasky, D. A.; Nesvizhskii, A. I. Fast Quantitative Analysis of timsTOF PASEF Data with MSFragger and IonQuant. *Mol Cell Proteomics* **2020**, *19* (9), 1575-1585. DOI: 10.1074/mcp.TIR120.002048 From NLM Medline.
(32) Brotzel, F.; Mayr, H. Nucleophilicities of amino acids and peptides. *Org Biomol Chem* **2007**, *5* (23), 3814-3820. DOI: 10.1039/b713778h From NLM Medline.
(33) Walkley, S. U.; Suzuki, K. Consequences of NPC1 and NPC2 loss of function in mammalian neurons. *Biochim Biophys Acta* **2004**, *1685* (1-3), 48-62. DOI: 10.1016/j.bbalip.2004.08.011 From NLM Medline.
(34) Chai, T.; Loh, K. M.; Weissman, I. L. TMX1, a disulfide oxidoreductase, is necessary for T cell function through regulation of CD3zeta. *bioRxiv* **2024**. DOI: 10.1101/2024.09.22.614388 From NLM PubMed-not-MEDLINE.
(35) Backus, K. M.; Correia, B. E.; Lum, K. M.; Forli, S.; Horning, B. D.; González-Páez, G. E.; Chatterjee, S.; Lanning, B. R.; Teijaro, J. R.; Olson, A. J.; et al. Proteome-wide covalent ligand discovery in native biological systems. *Nature* **2016**, *534* (7608), 570-+. DOI: 10.1038/nature18002.
(36) Guna, A.; Stevens, T. A.; Inglis, A. J.; Replogle, J. M.; Esantsi, T. K.; Muthukumar, G.; Shaffer, K. C. L.; Wang, M. L.; Pogson, A. N.; Jones, J. J.; et al. MTCH2 is a mitochondrial outer membrane protein insertase. *Science* **2022**, *378* (6617), 317-322. DOI: 10.1126/science.add1856.
(37) Gosney, J. A.; Wilkey, D. W.; Merchant, M. L.; Ceresa, B. P. Proteomics reveals novel protein associations with early endosomes in an epidermal growth factor-dependent manner. *J Biol Chem* **2018**, *293* (16), 5895-5908. DOI: 10.1074/jbc.RA117.000632 From NLM Medline.
(38) Yamamoto, H.; Koga, H.; Katoh, Y.; Takahashi, S.; Nakayama, K.; Shin, H. W. Functional Cross-Talk between Rab14 and Rab4 through a Dual Effector, RUFY1/Rabip4. *Mol Biol Cell* **2010**, *21* (15), 2746-2755. DOI: 10.1091/mbc.E10-01-0074.
(39) Cormont, M.; Mari, M.; Galmiche, A.; Hofman, P.; Le Marchand-Brustel, Y. A FYVE-finger-containing protein, Rabip4 is a Rab4 effector involved in early endosomal traffic. *P Natl Acad Sci USA* **2001**, *98* (4), 1637-1642. DOI: DOI 10.1073/pnas.031586998.
(40) Mari, M.; Macia, E.; Le Marchand-Brustel, Y.; Cormont, M. Role of the FYVE finger and the RUN domain for the subcellular localization of Rabip4. *Journal of Biological Chemistry* **2001**, *276* (45), 42501-42508. DOI: DOI 10.1074/jbc.M104885200.
(41) Char, R.; Pierre, P. The RUFYs, a Family of Effector Proteins Involved in Intracellular Trafficking and Cytoskeleton Dynamics. *Front Cell Dev Biol* **2020**, *8*. DOI: ARTN 779
10.3389/fcell.2020.00779.
(42) Yang, H. B.; Kim, O.; Wu, J.; Qiu, Y. Interaction between tyrosine kinase Etk and a RUN domain- and FYVE domain-containing protein RUFY1 - A possible role of Etk in regulation of vesicle trafficking. *Journal of Biological Chemistry* **2002**, *277* (33), 30219-30226. DOI: 10.1074/jbc.M111933200.
(43) Bissig, C.; Gruenberg, J. ALIX and the multivesicular endosome: ALIX in Wonderland. *Trends Cell Biol* **2014**, *24* (1), 19-25. DOI: 10.1016/j.tcb.2013.10.009.
(44) Larios, J.; Mercier, V.; Roux, A.; Gruenberg, J. ALIX- and ESCRT-III-dependent sorting of tetraspanins to exosomes. *J Cell Biol* **2020**, *219* (3). DOI: ARTN e201904113

10.1083/jcb.201904113.
(45) Gilis, D.; Massar, S.; Cerf, N. J.; Rooman, M. Optimality of the genetic code with respect to protein stability and amino-acid frequencies. *Genome Biol* **2001**, *2* (11), RESEARCH0049. DOI: 10.1186/gb-2001-2-11-research0049 From NLM Medline.
(46) Bar-Peled, L.; Kemper, E. K.; Suciu, R. M.; Vinogradova, E. V.; Backus, K. M.; Horning, B. D.; Paul, T. A.; Ichu, T. A.; Svensson, R. U.; Olucha, J.; et al. Chemical Proteomics Identifies Druggable Vulnerabilities in a Genetically Defined Cancer. *Cell* **2017**, *171* (3), 696-709 e623. DOI: 10.1016/j.cell.2017.08.051 From NLM Medline.
(47) Kemper, E. K.; Zhang, Y.; Dix, M. M.; Cravatt, B. F. Global profiling of phosphorylation-dependent changes in cysteine reactivity. *Nat Methods* **2022**, *19* (3), 341-352. DOI: 10.1038/s41592-022-01398-2 From NLM Medline.
(48) Zhai, Y.; Zhang, X.; Chen, Z.; Yan, D.; Zhu, L.; Zhang, Z.; Wang, X.; Tian, K.; Huang, Y.; Yang, X.; et al. Global profiling of functional histidines in live cells using small-molecule photosensitizer and chemical probe relay labelling. *Nat Chem* **2024**. DOI: 10.1038/s41557-024-01545-6.
(49) Takeuchi, H.; Takada, A.; Kuboniwa, M.; Amano, A. Intracellular periodontal pathogen exploits recycling pathway to exit from infected cells. *Cell Microbiol* **2016**, *18* (7), 928-948. DOI: 10.1111/cmi.12551.
(50) Liss, V.; Swart, A. L.; Kehl, A.; Hermanns, N.; Zhang, Y.; Chikkaballi, D.; Bohles, N.; Deiwick, J.; Hensel, M. Salmonella enterica Remodels the Host Cell Endosomal System for Efficient Intravacuolar Nutrition. *Cell Host Microbe* **2017**, *21* (3), 390-402. DOI: 10.1016/j.chom.2017.02.005 From NLM Medline.
(51) Kyei, G. B.; Vergne, I.; Chua, J.; Roberts, E.; Harris, J.; Junutula, J. R.; Deretic, V. Rab14 is critical for maintenance of
phagosome maturation arrest. *Embo J* **2006**, *25* (22), 5250-5259. DOI: 10.1038/sj.emboj.7601407.
(52) Kelley, V. A.; Schorey, J. S. 's arrest of phagosome maturation in macrophages requires Rab5 activity and accessibility to iron. *Mol Biol Cell* **2003**, *14* (8), 3366-3377. DOI: DOI 10.1091/mbc.E02-12-0780.